


RESEARCH ARTICLE

Pressure-assisted cooling to grow ultra-stable $\text{Cs}_3\text{Cu}_2\text{I}_5$ and CsCu_2I_3 single crystals for solid-state lighting and visible light communication

Baiqian Wang¹ | Chen Chen² | Xin Yang¹ | Wensi Cai¹ | Shuangyi Zhao¹ |
Ru Li¹ | Wen Ma¹ | Jiangzhao Chen¹ | Zhigang Zang¹ 

¹Key Laboratory of Optoelectronic Technology & Systems (Ministry of Education), Chongqing University, Chongqing, China

²School of Microelectronics and Communication Engineering, Chongqing University, Chongqing, China

Correspondence

Jiangzhao Chen, and Zhigang Zang, Key Laboratory of Optoelectronic Technology & Systems (Ministry of Education), Chongqing University, Chongqing, 400044, China.
Email: jiangzhaochen@cqu.edu.cn and zangzg@cqu.edu.cn

Funding information

Fundamental Research Funds for the Central Universities, Grant/Award Number: 2021CDJQY-022; National Natural Science Foundation of China, Grant/Award Numbers: 11974063, 61904023; Natural Science Foundation of Chongqing, Grant/Award Number: cstc2019jcyj-bshX0078

Abstract

Owing to the excellent optical properties, white light-emitting diodes (WLEDs) based on metal halide perovskites have attracted great attention as promising light source for solid-state lighting and wireless visible light communication (VLC). However, the instability and toxicity of classic hybrid lead halides hinder their practical applications. Here, a pressure-assisted cooling method is developed to grow lead-free $\text{Cs}_3\text{Cu}_2\text{I}_5$ and CsCu_2I_3 single crystals, which exhibit more excellent stability, larger size and uniform orientations in comparison with pressure-free cooling method. Then, both single crystals are used as the emitters of WLEDs without encapsulation, exhibiting a high Color Rendering Index of 91, a decent Commission Internationale de l'Eclairage coordinate of (0.33, 0.33), a proper Correlated Color Temperature of 5436 K, as well as an excellent 1350-h operating stability at atmosphere. Furthermore, the prepared WLEDs are utilized in wireless VLC, which possesses a -3 dB bandwidth of 10.1 MHz.

KEYWORDS

$\text{Cs}_3\text{Cu}_2\text{I}_5$, CsCu_2I_3 , single crystals, visible light communication (VLC), white light-emitting diodes (WLEDs)

1 | INTRODUCTION

Due to the excellent defect tolerance, high photoluminescence quantum yield (PLQY), high absorption coefficients and tunable band gap, metal halide perovskites have been widely demonstrated to be outstanding light-emitting materials for light-emitting diodes (LEDs).^{1–5} However, for classic lead halide perovskites, their toxicity of lead elements have been reported to impede their development in commercialization.^{6–10}

Consequently, lead-free halide perovskites are desirable in promoting the development of optoelectronic devices, including solar cells,¹¹ white light-emitting diodes (WLEDs),^{12–14} photodetectors^{15–17} and X-ray scintillators.^{18–20} Among all lead-free halide perovskites, inorganic copper halide perovskites have been explored as excellent candidates for highly efficient WLEDs²¹ and detectors.²² Due to the strong self-trapped excitons (STEs) effect, copper halides perovskites exhibit large Stokes shifts, broad

This is an open access article under the terms of the Creative Commons Attribution License, which permits use, distribution and reproduction in any medium, provided the original work is properly cited.

© 2022 The Authors. *EcoMat* published by The Hong Kong Polytechnic University and John Wiley & Sons Australia, Ltd.

photoluminescence (PL) spectra, high PLQY and long PL decay time, which result in efficient WLEDs.²³ Recently, inorganic copper halide perovskites have been successfully employed to prepare WLEDs.²⁴ Zang et al.²⁵ and Shan et al.²⁶ prepared WLEDs based on inorganic copper halide nanocrystals and thin films, respectively. However, the low operation stability (the lifetime of emission intensity decline to 50% of its initial value is 10^0 – 10^1 h (h)) impedes the further development of WLEDs. Such instability generally results from the oxidation and decomposition of copper halide perovskites when exposing to moisture and high temperature.²⁵

To enhance the stability, one feasible and effective strategy is to prepare bulk copper halide perovskites, that is, single crystals, to decrease specific surface area of materials. Up to now, several works on copper halide single crystals have been reported, in which the single crystals are prepared by an anti-solvent method.^{27–30} For example, Hosono et al. prepared a $\text{Cs}_3\text{Cu}_2\text{I}_5$ single crystal with a size of 2×5 mm, exhibiting a broad PL peak centered at 445 nm and a high PLQY of 91.2%.²⁹ Huang et al. grew a rod-like CsCu_2I_3 single crystal with a size of 10×1.5 mm at 60°C for 48 h, whose PL peak centers at 568 nm and PLQY is 15.7%.³⁰ However, due to the low solubility of precursors in organic solvents, the sizes of crystals prepared by the anti-solvent method are smaller than those prepared by the heating solution method and hydriodic acid (HI)-based precursor solution cooling method, since the high temperature and hydrous HI can facilitate the dissolution of precursor materials.³¹ In addition, the morphology and surface of single crystals grown by the anti-solvent method are irregular and uneven due to the uncontrollable growth rate, resulting in degradation of the corresponding single crystal perovskite optoelectronic devices.³² Thus, it is quite urgent to grow large copper halide single crystals with excellent morphology and optoelectronic properties through developing more effective single crystal growth method.³³

In this work, we developed a pressure-assisted cooling method to grow $\text{Cs}_3\text{Cu}_2\text{I}_5$ and CsCu_2I_3 single crystals for WLEDs and wireless visible light communication (VLC) systems. The precursors dissolved in HI were first heated to reach their super-solubility, and then the saturated solution was filtered to remove the micro crystals, followed by a slow cooling speed of $1^\circ\text{C}/\text{h}$ to room temperature. Owing to the filtering and slow cooling, the large single crystals with improved uniform orientation were prepared and showed enhanced optoelectronic properties. The as-synthetic $\text{Cs}_3\text{Cu}_2\text{I}_5$ and CsCu_2I_3 single crystals exhibited broad PL spectra centered at 444 and 580 nm with high PLQY values of 99.75% and 16.73%, respectively. Apart from the optical performance,

excellent stability was also demonstrated for the $\text{Cs}_3\text{Cu}_2\text{I}_5$ and CsCu_2I_3 single crystals. Due to the broadband emission, high PLQY as well as stability, the WLEDs without encapsulation exhibited a high color rendering index (CRI) of 91 and a 1350-h operating stability at atmosphere. Moreover, the high-performance WLEDs were applied in wireless VLC systems, in which the -3 dB bandwidth and the achievable data rate using orthogonal frequency division multiplexing (OFDM) modulation were 10.1 MHz and 87.7 Mbps, respectively. The excellent performance of lighting and communication of WLEDs using $\text{Cs}_3\text{Cu}_2\text{I}_5$ and CsCu_2I_3 clearly demonstrate the advantages of $\text{Cs}_3\text{Cu}_2\text{I}_5$ and CsCu_2I_3 single crystals, which can promote the development of copper halide perovskites and extend their practical applications in other optoelectronic fields.

2 | RESULTS AND DISCUSSION

2.1 | Preparation of cesium copper iodine single crystals

As shown in Figure 1A, a pressure-assisted HI-based precursor solution cooling method was used to synthesize $\text{Cs}_3\text{Cu}_2\text{I}_5$ and CsCu_2I_3 single crystals, in which the heating precursor solution was filtered to remove the white precipitate. Then the saturated solution is injected into the poly(tetrafluoroethylene) lining of the reactor and heating again, resulting in the formation of a crystal nucleus with corresponding critical nucleation radii. With a slow cooling speed of $1^\circ\text{C}/\text{h}$ (from 100°C to room temperature), the solubility of precursors solution reduced, leading to the spontaneous growth of the little crystal nucleus and resulting in a separation of the precursors solution to facilitate the enlarge of crystal sizes instead of dissolution of as-grew crystals. The growth process of pressure-free cooling method is the same as that of pressure-assisted cooling method, and the difference is that its container is a common glass bottle in pressure-free cooling method. Compared with the copper halides single crystals prepared by pressure-free cooling method and the anti-solvent method,^{27–30} the $\text{Cs}_3\text{Cu}_2\text{I}_5$ and CsCu_2I_3 single crystals prepared by the pressure-assisted cooling method exhibit larger sizes of 7×6 mm and 16×3 mm, respectively, as shown in Figure 1B,C. In addition to the larger sizes, $\text{Cs}_3\text{Cu}_2\text{I}_5$ and CsCu_2I_3 single crystals grown with pressure-assisted show excellent crystallinity and morphology, compared to pressure-free cooling method, which were confirmed by the characterization results of X-ray diffraction (XRD) and thermogravimetric (TG) analysis (Figure S1). Figure 1D,E shows the XRD results of $\text{Cs}_3\text{Cu}_2\text{I}_5$ and CsCu_2I_3 crystals

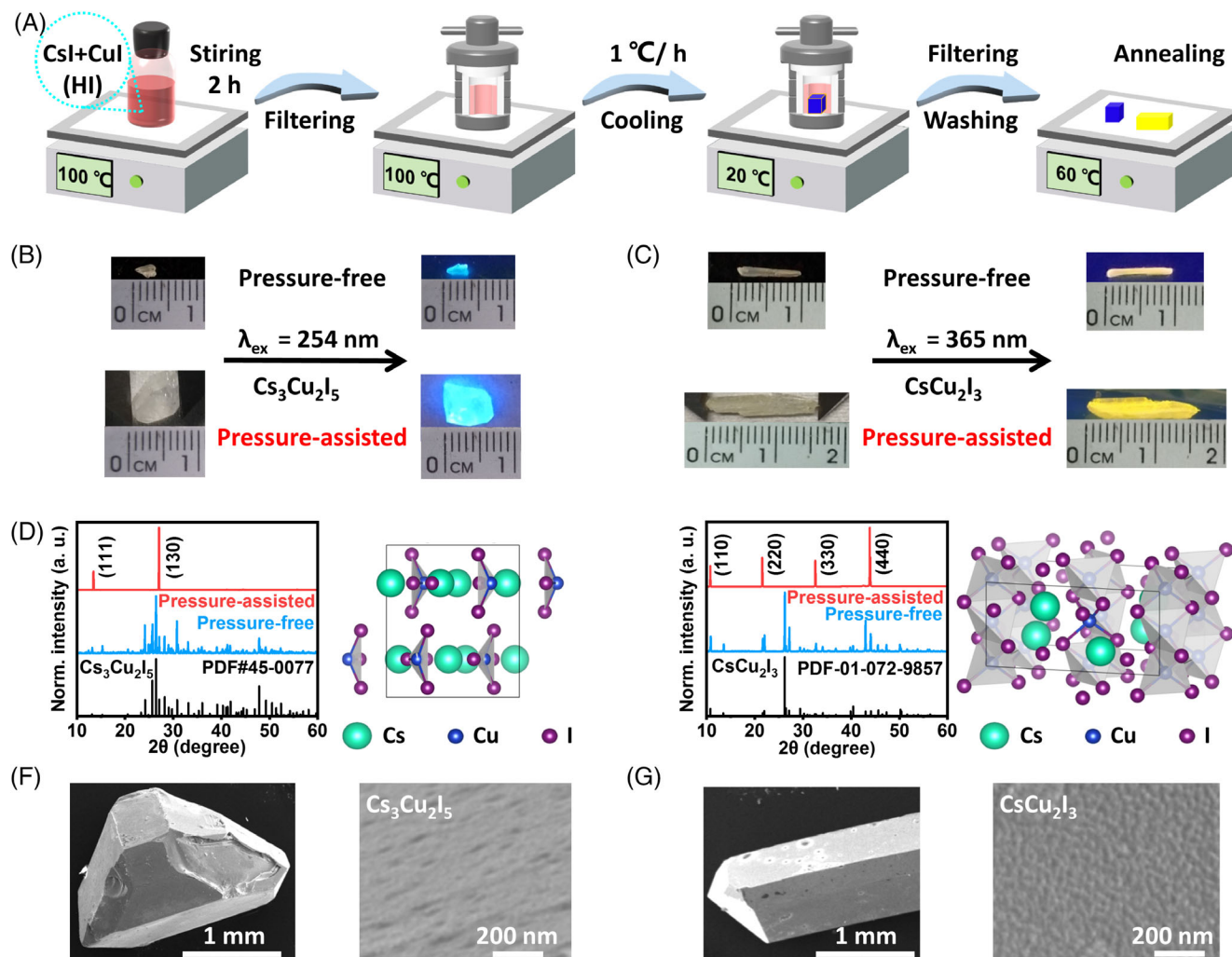


FIGURE 1 (A) Schematically illustrated diagram of grown process of $\text{Cs}_3\text{Cu}_2\text{I}_5$ and CsCu_2I_3 single crystals; (B) photographs of $\text{Cs}_3\text{Cu}_2\text{I}_5$ and (C) CsCu_2I_3 single crystals grown with pressure-free and pressure-assisted; (D) XRD patterns and crystal structures of $\text{Cs}_3\text{Cu}_2\text{I}_5$ and (E) CsCu_2I_3 single crystals grown with pressure-assisted. (F) Scanning electron microscopy (SEM) images of $\text{Cs}_3\text{Cu}_2\text{I}_5$ and (G) CsCu_2I_3 single crystals grown with pressure-assisted

grown with pressure-free and pressure-assisted, respectively, in which the narrow full width at half maxima (FWHM) and large diffraction intensity demonstrate their good crystallinity. Furthermore, the existence of specific diffraction peaks illustrated oriented surface, which is regarded as a single-crystal nature. The elements states of both single crystals was proved by X-ray photoelectron spectroscopy (XPS) (Figures S2 and S3), in which the presence of Cs^+ , Cu^+ , and I^- indicates not only their chemical components but also the negligible oxidation of monovalent copper ions. By analyzing the crystal structure (Table S1), the crystal systems of both single crystals grown with pressure-assisted are identified as orthorhombic, but cell units show $a = 10.1749 \text{ \AA}$, $b = 11.6476 \text{ \AA}$, $c = 14.3540 \text{ \AA}$, $\alpha = \beta = \gamma = 90^\circ$ and $a = 10.3268 \text{ \AA}$, $b = 13.3406 \text{ \AA}$, $c = 6.2206 \text{ \AA}$, $\alpha = \beta = \gamma = 90^\circ$ for $\text{Cs}_3\text{Cu}_2\text{I}_5$ and CsCu_2I_3 crystals, respectively. The basic units of $\text{Cs}_3\text{Cu}_2\text{I}_5$ are $[\text{Cu}_2\text{I}_5]^{3-}$ dimers, including edge-

connected $[\text{CuI}_4]^{3+}$ tetrahedra and $[\text{CuI}_3]^{2-}$ triangles, which are separated by Cs^+ ions, leading to a zero-dimensional crystal configuration of $\text{Cs}_3\text{Cu}_2\text{I}_5$. In contrast, CsCu_2I_3 contain numerous edge-shared $[\text{CuI}_4]^{3-}$ tetrahedra and isolated Cs^+ ions, leading to the formation of one-dimensional chain-like sharp.³⁴ Thus, owing to the differences between crystal structures and configuration of both copper halide single crystals, their sizes, sharps and luminescence under ultraviolet excitation are distinguishing. However, the prepared single crystals from the pressure-assisted cooling method possess uniform orientation and smooth surface, as shown in Figure 1F,G. It may indicate that the optimized preparation methods can facilitate the growth of $\text{Cs}_3\text{Cu}_2\text{I}_5$ and CsCu_2I_3 single crystals with large sizes and excellent morphologies, improving their optoelectronic performance. Besides, regular surface of both crystals grown with pressure-assisted also checked with PL mapping images in

Figure S4. PL mapping results were collected under a 325 nm pump excitation, which images indicate the uniform distribution of components and low defect density, implying the feasibility and advantages of our optimized single-crystal preparation method.

2.2 | Optical properties of cesium copper iodine single crystals

Figure 2 shows the optical properties of $\text{Cs}_3\text{Cu}_2\text{I}_5$ and CsCu_2I_3 single crystals grown with pressure-free and pressure-assisted methods. As shown in Figure 2A, the $\text{Cs}_3\text{Cu}_2\text{I}_5$ single crystals grown by the both methods exhibit the similar PL spectra with peaks at 444 nm. It is worth noting that the pressure-assist method facilitates to enhance the PLQY of single crystals from 85.16% to 99.75%, compared with the pressure-free growth method. In addition, the PL decay time of the $\text{Cs}_3\text{Cu}_2\text{I}_5$ single crystals grown by the pressure-assisted method is found to vary from 1017.71 to 1072.38 ns (Figure 2B and Table S2), implying the increase of radiative recombination rates induced by the reduction of defects. Similarly, benefiting from the optimum effect of the pressure-assisted method, the CsCu_2I_3 single crystals prepared by the strategy show enhanced PLQY of 16.73% and PL decay time of 52.99 ns (Table S2), as shown in Figure 2C,D. The lifetime (τ) is

defined as the average time of carrier existence, which is calculated by equation as following³⁵:

$$\frac{1}{\tau} = \frac{1}{\tau_{\text{non}}} + \frac{1}{\tau_{\text{rad}}}$$

where the τ_{non} and τ_{rad} is non-radiative and radiative life-time, respectively.

To clarify the photoluminescent mechanism of $\text{Cs}_3\text{Cu}_2\text{I}_5$ and CsCu_2I_3 single crystals grown with pressure-assisted, the PLE-dependent PL spectra were measured. With the evolution of excitation wavelength, the normalized (Norm.) PL intensity of both single crystals changes in Figure S5, but no obvious shifts of PL spectra is found. This phenomenon illustrates that the luminescent centers of both single crystals may not change with the different excitation light. In addition, as shown in Figure S6, with the enlargement of excitation power, the PL intensity of both crystals enhances constantly, implying that the luminescence does not originate from the defects in these crystals. Because of the PL intensity will eventually saturate when all defects are filled by carriers. Therefore, the luminescent mechanism is expected to derive from the effect of STEs. Besides, the PL spectra of both single crystals grown with pressure-assisted exhibit large Stokes shifts, broad PL FWHM (Figure 3A,D) and long PL decay time (Figure 2B,D),

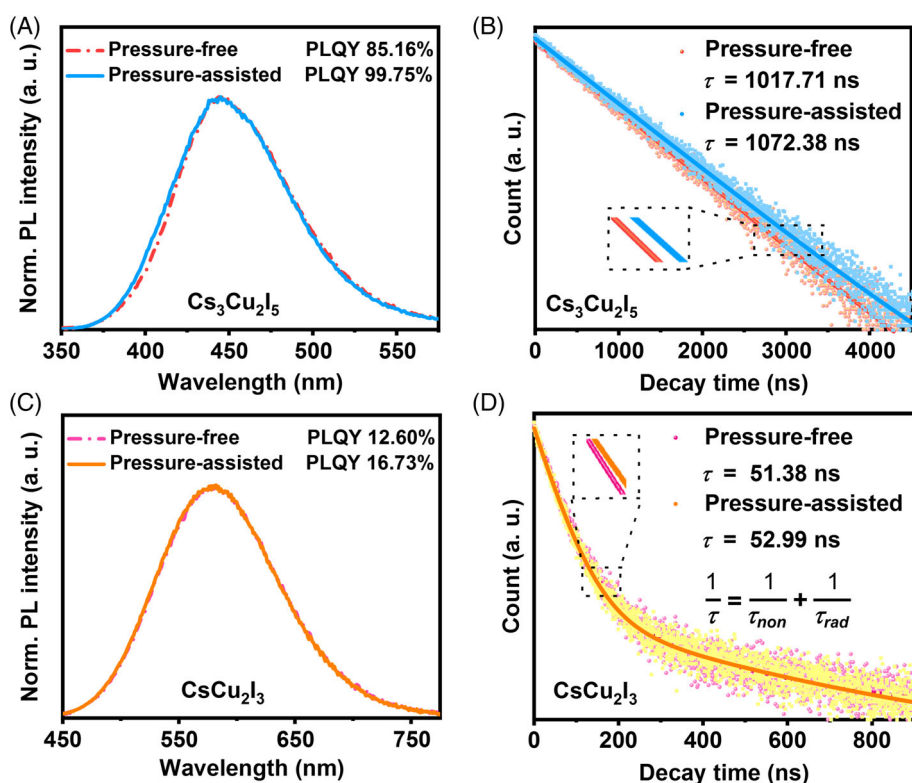


FIGURE 2 (A) Photoluminescence (PL) and (B) transient PL decay curves of the $\text{Cs}_3\text{Cu}_2\text{I}_5$ single crystals grown by pressure-free and pressure-assisted methods, respectively; (C) PL and (D) transient PL decay curves of the CsCu_2I_3 single crystals grown by pressure-free and pressure-assisted methods, respectively

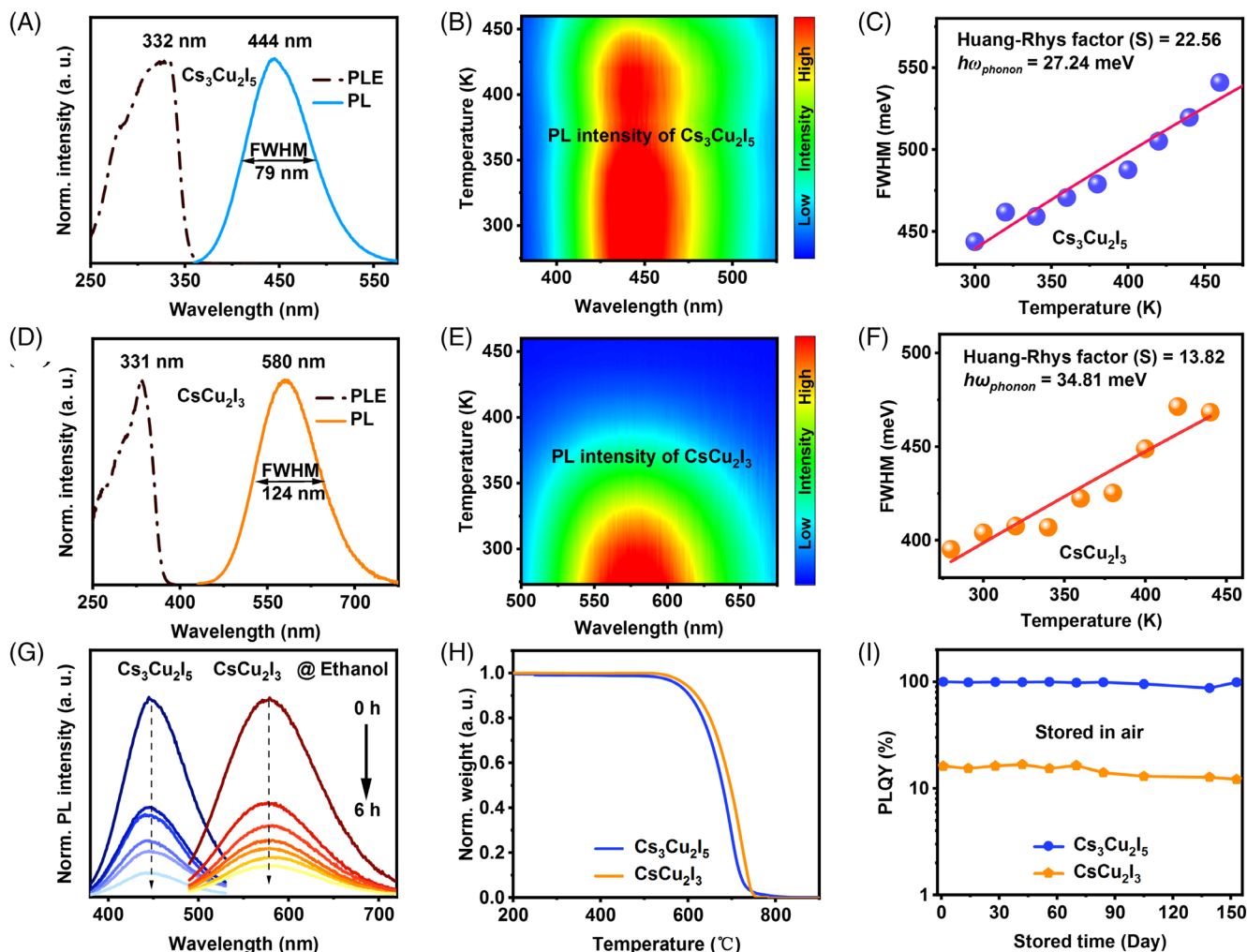


FIGURE 3 (A) Photoluminescence excitation (PLE) and (B) PL Contour mapping of temperature-dependent PL spectra excited at 330 nm and (C) FWHM of the PL spectra as a function of measuring temperature of the $\text{Cs}_3\text{Cu}_2\text{I}_5$ single crystals; (D) PLE and (E) PL Contour mapping of temperature-dependent PL spectra excited at 330 nm, and (F) FWHM of the PL spectra as a function of measuring temperature of the CsCu_2I_3 single crystals. (G) PL spectra of $\text{Cs}_3\text{Cu}_2\text{I}_5$ and CsCu_2I_3 single crystals with adding of ethanol. (H) Thermogravimetric curves of both single crystals. (I) Change of PLQY of $\text{Cs}_3\text{Cu}_2\text{I}_5$ and CsCu_2I_3 single crystals grown with pressure-assisted method

which may be attributed to the effects of STEs.^{36–39} Furthermore, the temperature-dependent PL characterization was performed to confirm the existence of STEs in both copper halide single crystals. Negligible change of PL peaks was found with the increase of measuring temperature from 273 to 460 K, as shown in Figure 3B,E. However, the PL intensity reduces with enhanced temperature, which is owing to the enhanced exciton-phonon coupling at low temperatures and severe thermal quenching at high temperatures. The origin of STEs is the exciton-phonon coupling, which can be evaluated by the Huang-Rhys factor (S) and the phonon frequency ($\hbar\omega_{\text{phonon}}$) through the following equation⁴⁰:

$$\text{FWHM} = 2.36\sqrt{S\hbar\omega_{\text{phonon}}}\sqrt{\coth\frac{\hbar\omega_{\text{phonon}}}{2k_{\text{B}}T}},$$

where the k_{B} is Boltzmann constant and T is temperature. By fitting the FWHM and temperature, the S and $\hbar\omega_{\text{phonon}}$ are calculated as 22.56 and 27.24 meV for the $\text{Cs}_3\text{Cu}_2\text{I}_5$ crystal, as shown in Figure 3C. For the CsCu_2I_3 single crystal, the calculated S and $\hbar\omega_{\text{phonon}}$ are 13.82 and 34.81 meV, respectively (Figure 3F). The large S and $\hbar\omega_{\text{phonon}}$ results clarify the strong exciton-phonon coupling in both copper halide single crystals, implying the presence the STEs effects and demonstrating that the enhancement of PL intensity in lower measuring ranges is indeed due to the improved exciton-phonon coupling

and amounts of STEs, instead of the conventional band-edge emission.

Apart from the prominent optical performance, the excellent stability, including anti-polar-solvent, thermal stability, and air stability, is found for the $\text{Cs}_3\text{Cu}_2\text{I}_5$ and CsCu_2I_3 single crystals grown with pressure-assisted. As shown in Figure 3G, by adding ethanol as a polar solvent, the normalized PL intensity of both single crystals reduce, but the PL intensity of the CsCu_2I_3 single crystal is greater than that of the $\text{Cs}_3\text{Cu}_2\text{I}_5$ crystal after 6 h. Thus, it is inferred that the CsCu_2I_3 single crystal with one-dimensional chain-like configuration is more stable against polar solvents. Furthermore, the high-temperature stability of both single crystals was investigated via measuring TG. As shown in Figure 3H, the stable temperatures (without decomposition) of $\text{Cs}_3\text{Cu}_2\text{I}_5$ and CsCu_2I_3 single crystals are up to 576 and 594°C (weight loss 5%), respectively. As the heating temperature furtherly enhances, the weights of $\text{Cs}_3\text{Cu}_2\text{I}_5$ or CsCu_2I_3 single

crystals are found to reduce gradually, suggesting the evaporation of both crystals into the gaseous state at higher temperature. Finally, Figure 3I shows the change of PLQY for both single crystals stored in air. It is found that their PLQY values are maintained after the 153-day storage in air, indicating the excellent stability of inorganic copper halide single crystals.

2.3 | Applications of cesium copper iodine single crystals

2.3.1 | White lighting

To explore the potential optoelectronic applications of the inorganic lead-free $\text{Cs}_3\text{Cu}_2\text{I}_5$ and CsCu_2I_3 single crystals grown with pressure-assisted method, WLEDs were prepared via a simple paste technique. Both crystals with an optimized ratio (Figure S7) were pasted to the

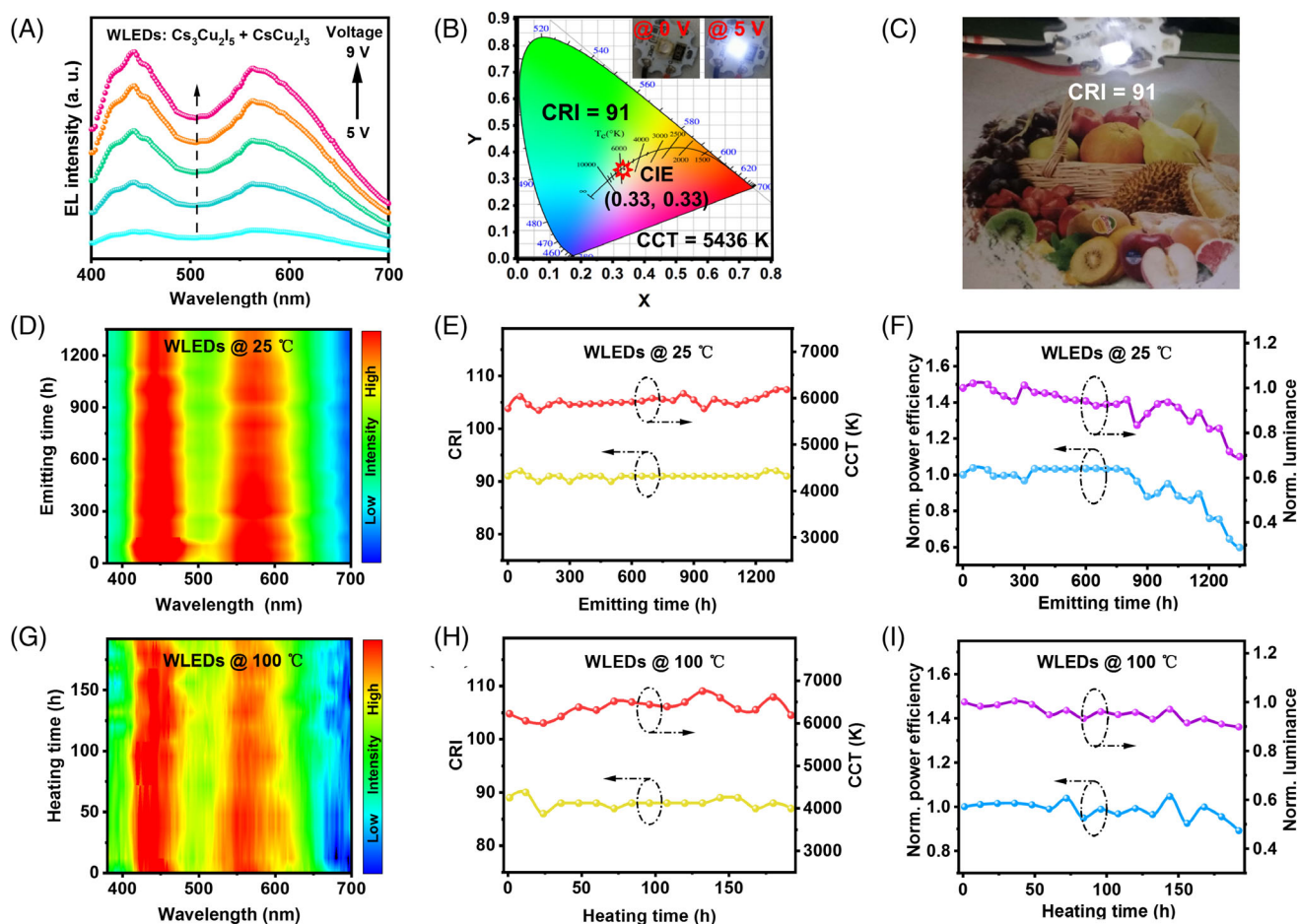


FIGURE 4 (A) EL spectra of as-prepared WLEDs with $\text{Cs}_3\text{Cu}_2\text{I}_5$ and CsCu_2I_3 single crystals. (B) CIE chromaticity diagram of the prepared WLEDs. The inset is a photo with the WLEDs turned off and on; (C) Photographs of the operating WLEDs (CRI = 91) obtained under darkroom; (D) Contour mapping of the EL spectra; (E) Evolution of CRI and CCT; (F) Changes of normalized power efficiency and luminance of WLEDs operating during 1350-h at atmosphere; (G) Contour mapping of the EL spectra; (H) Evolution of CRI and CCT; (I) Changes of normalized power efficiency and luminance of WLEDs operating during 192-h at 100°C

commercial UV chips (300 nm) without encapsulation, leading to a broad electroluminescence (EL) spectra including two peaks of $\text{Cs}_3\text{Cu}_2\text{I}_5$ and CsCu_2I_3 . As shown in Figure 4A, the EL intensity is boosted with the enhancement of driving voltages on WLEDs. The WLEDs exhibit a highest CRI of 91, a decent CIE color coordinate of (0.33, 0.33) and a moderate CCT of 5436 K (Figure 4B), which can act as excellent light sources to exhibit the real color of an object,⁴¹ as shown in Figure 4C. In addition to the high luminous performance, WLEDs based on the $\text{Cs}_3\text{Cu}_2\text{I}_5$ and CsCu_2I_3 single crystals show excellent stability under both atmosphere and high temperature. Figure 4D shows the evolution of EL spectra during 1350-h continuous operation at atmosphere, where no obvious changes of EL intensity and shifts of EL peaks are found, as well as CRI and CCT (Figure 4E). Although the power efficiency and luminance are found to reduce continually, they maintain almost 60% of their initial values after 1350-h operation, confirming the long time operating stability of WLEDs (Figure 4F). Besides, as shown in Figure 4G–I, negligible changes are found in the EL spectra of WLEDs at 100°C with a slight evaluate of CRI, CCT, power efficiency and luminance after 192 h, owing to the thermal quenching. It may imply the

excellent operating stability of WLEDs at high temperature is due to the good stability of both single crystals. The maintained deviation of WLEDs both at atmosphere and high temperature suggests the potentials of WLEDs as promising light sources (Figure S7). Compared with the reported work, our WLED has huge advantages in terms of CRI and stability in Table 1.

2.3.2 | Wireless visible light communication

Furthermore, the prepared WLEDs could be applied as light sources in wireless VLC systems, as shown in Figure 5A. Under the excitation, the WLEDs emit white light as carriers of the information, which is detected by photodetectors. Figure 5B shows the measured electrical-optical-electrical (EOE) frequency response of the system, where a high -3 dB bandwidth of 10.1 MHz can be obtained and the inset showing the captured 10-MHz eye diagram. This bandwidth is higher than that of published WLEDs (< 2 MHz).^{6,25,53} Figure 5C exhibits the received signal-to-noise ratio (SNR) of the system with a modulation bandwidth of 20 MHz, showing a high SNR of more than 16 dB above the -3 dB bandwidth. To fully explore

TABLE 1 Comparison of WLEDs with the published literatures

Emitter	Structure	Components	CRI	CIE	CCT (K)	Stability	Ref.
CsPbBr_3	3D	Quantum dots + Phosphor	91	(0.40, 0.41)	3689	/	42
MAPbX_3	3D	Perovskite + Phosphor	85	(0.31, 0.34)	6581	/	43
Gd^{3+} doped CsPbBrI_2	3D	Nanocrystals	81	(0.33, 0.34)	5430	/	44
Sm^{3+} doped CsPbCl_3	3D	Nanocrystals	93	(0.32, 0.31)	/	1464 h ($> 30\%$)	45
$\text{CsPbBr}_3 + \text{Mn}^{2+}$ doped $\text{PEA}_2\text{PbBr}_4$	3D	Nanoplatelets + nanosheets	90	(0.33, 0.33)	5677	/	46
α -(DMEN) PbBr_4	2D	Single crystals	73	(0.28, 0.36)	7863	/	47
(EDBE) PbBr_4	2D	Single crystals	84	(0.39, 0.42)	3990	/	48
(OCTAm) $_2\text{SnX}_4$	2D	crystalline + Phosphor	89	(0.33, 0.31)	6530	/	49
$\text{Cs}_2\text{Ag}_{1-x}\text{Na}_x\text{InCl}_6$	3D	Single crystals	/	(0.40, 0.45)	4054	1000 h ($> 95\%$)	14
Mn^{2+} doped K_3SbCl_6	0D	Nanocrystals	88	(0.35, 0.30)	5068	12 h ($> 50\%$)	50
$\text{CsCu}_2\text{Cl}_3/\text{Cs}_3\text{Cu}_2\text{Cl}_5$	1D/0D	Nanocrystals + Phosphor	94	(0.34, 0.34)	5285	60 h ($> 64\%$)	51
$(\text{C}_4\text{N}_2\text{H}_{14}\text{Br})_4\text{SnBr}_6$	0D	Single crystals + Phosphor	70	(0.35, 0.39)	4946	/	52
$\text{Cs}_2\text{InCl}_5 \cdot \text{H}_2\text{O} \cdot \text{Sb}^{3+}$	0D	Blue chip + Single crystals	86	(0.34, 0.36)	4556	/	40
$\text{Cs}_3\text{Cu}_2\text{I}_5/\text{CsCu}_2\text{I}_3$	0D/1D	Single crystals	91	(0.33, 0.33)	5436	1350 h ($> 60\%$)	This work

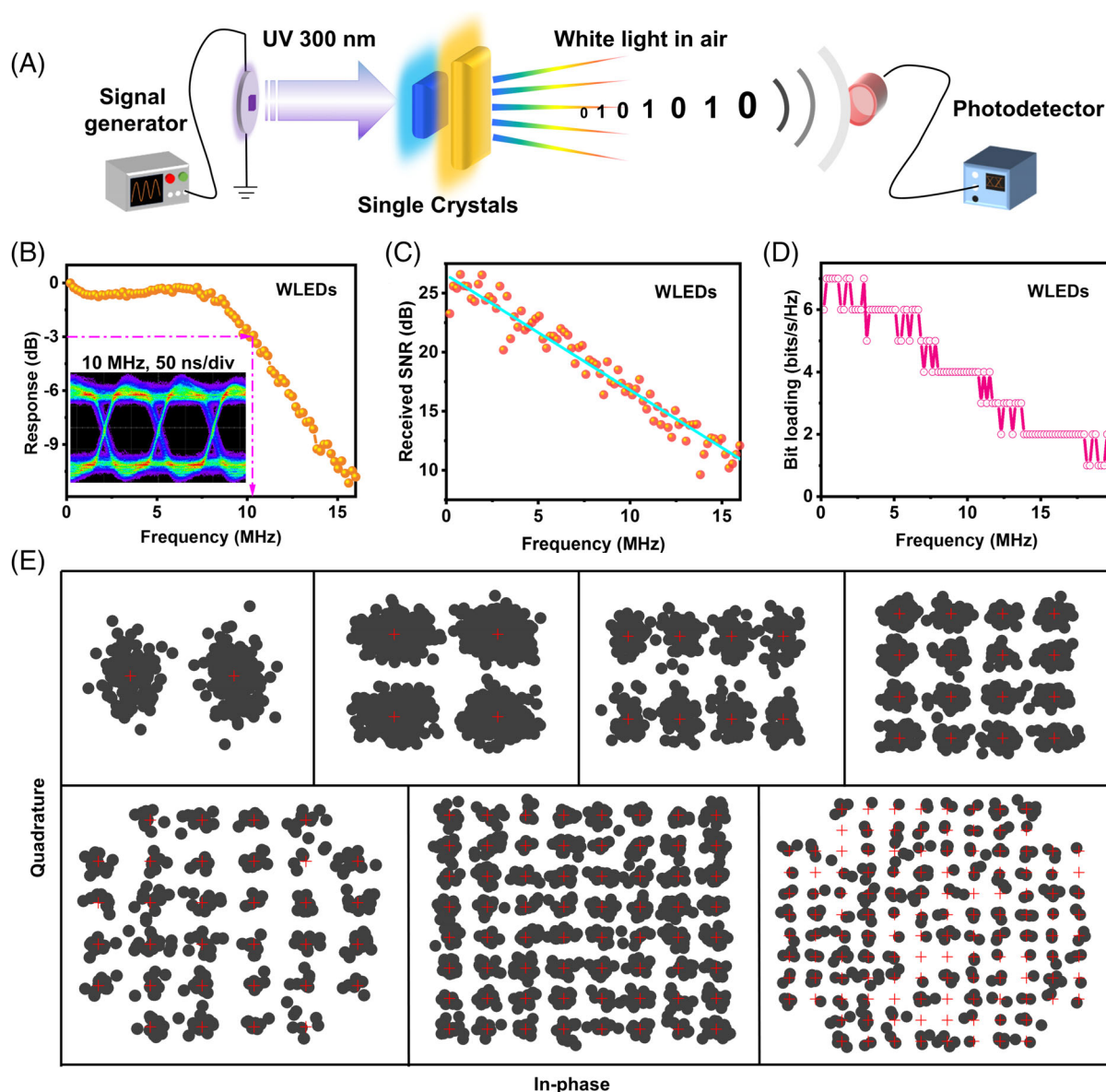


FIGURE 5 (A) Experimental setup of the visible light communication system by WLEDs; (B) EOE frequency response with the inset showing the captured eye diagram; (C) received SNR; (D) bit loading profile using OFDM modulation, and (E) the corresponding constellation diagrams of binary phase shift keying (BPSK), 4QAM, 8QAM, 16QAM, 32QAM, 64QAM, and 128QAM, respectively

the achievable data rate, we applied OFDM modulation with adaptive bit loading in the system. Figure 5D shows the resultant bit loading profile, in which as high as 7 bits/s/Hz can be loaded to the subcarriers within the low frequency region. As a result, the achievable data rate can reach 87.7 Mbps and the corresponding constellation diagrams, including the binary phase shift keying (BPSK), 4-ary quadrature amplitude modulation (QAM), 8QAM, 16QAM, 32QAM, 64QAM, and 128QAM be found in Figure 5E. The achievable data rate of the OFDM modulation is obtained by the equation of $R = B \log_2(M)$, where B is the modulation

bandwidth of the OFDM signal and M is the achievable maximum QAM constellation.⁵⁴

3 | CONCLUSION

In summary, we have demonstrated a pressure-assisted HI-based precursors solution cooling method for preparing $\text{Cs}_3\text{Cu}_2\text{I}_5$ and CsCu_2I_3 single crystals, exhibiting large sizes, uniform orientation and smooth surface, which leads to enhanced optical performance and stability against polar solvents and heat. These PL mechanisms of

both crystals are attributed to the STEs, and the optical properties are feasible for preparation of WLEDs. The resulted WLEDs exhibit a high CRI of 91 and an excellent CIE coordinate of (0.33, 0.33), as well as an ultra-stable operation at atmosphere and high temperatures. Furthermore, the prepared WLEDs may act as the light sources of wireless VLC systems, in which a -3 dB bandwidth of 10.1 MHz and a high data rate of 87.7 Mbps can be achieved, indicating the promising potential of copper halide single crystals in various optoelectronic applications.

4 | EXPERIMENTAL SECTION

4.1 | Materials

Cesium iodide (CsI, 99.9%) and Hydroiodic acid (HI, 45%–50%) were purchased from Aladdin Chemistry Technology Co., Ltd. Cuprous iodide (CuI, 99.9%) was purchased from Macklin Inc.

4.2 | Single crystals growth

CsCu₂I₃: CsI (5 mmol), CuI (10 mmol), HI (20 ml), and Magnetron were added to a glass bottle. The mixture was stirred at 100°C for 2 h. Next, the white precipitate was removed by polytetrafluoroethylene (PTFE 0.45 μ m) filters and syringes, and the saturated solution was injected into the PTFE lining of the reactor. This reactor was placed in a heating table with 100°C. And then, the reactor was cooled to room temperature by 1°C/h. Finally, CsCu₂I₃ single crystals were obtained after filtering, washing and annealing.

Cs₃Cu₂I₅: CsI (15 mmol), CuI (10 mmol), HI (20 ml), and Magnetron were added to a glass bottle. The mixture was stirred at 100°C for 2 h. Next, the white precipitate was removed by polytetrafluoroethylene (PTFE 0.45 μ m) filters and syringes, and the saturated solution was injected into the PTFE lining of the reactor. This reactor was placed in a heating table with 100°C. After that, it was cooled to room temperature by 1°C/h. Finally, Cs₃Cu₂I₅ single crystals were obtained after filtering, washing and annealing.

The heating Table (JW-400) was purchased from Wuhan Junwei Technology Company. The single crystals grown by pressure-assisted cooling method used reactors, while the pressure-free cooling method for single crystals growth used glass bottles.

4.3 | Material characterization

The XRD results were collected by a PANalytical X' Pert Powder (Spectris Pte. Ltd, The Netherlands) with a Cu K α tube operated at 40 kV and 40 mA. The scanning electron

microscopy (SEM) images were collected with a tungsten filament scanning electron microscope Quattro S (Thermo Fisher Scientific Co., Ltd. USA). The XPS was measured by ESCALAB250Xi (Thermo Fisher Scientific Co., Ltd. USA). All the PLE/PL/PLQY/ τ were measured by FLS1000 (Edinburgh Instruments, England). The thermogravimetric and differential scanning calorimeter (TG-DSC) data was implemented on a TGA2 (Mettler Toledo, Switzerland).

PLQYs were measured with a FLS1000 fluorescence spectrometer with an integrating sphere attachment. The excitation and emission light from all directions of the sample surface were homogenized by the integrating sphere, and light at the exit port entered the monochromator for detection by the photodetector. First, test the PL spectrum *A* of a blank (without sample) by integrating sphere; then, test a PL spectrum *B* of the sample by integrating sphere; finally, use the following formula to obtain PLQY:

$$\text{PLQY} = \frac{E_B - E_A}{S_B - S_A}$$

where the E_A and S_A is the photon counts corresponding to emission wavelength (sphere background) and excitation wavelength of PL spectrum *A*. The E_B and S_B is the photon counts corresponding to emission wavelength and excitation wavelength of PL spectrum *B*. $\text{FWHM} = 2.36\sqrt{S}\hbar\omega_{\text{phonon}}\sqrt{\coth\frac{\hbar\omega_{\text{phonon}}}{2k_B T}}$

4.4 | Preparation and measurement of light-emitting diodes (LEDs)

All LEDs were prepared by paste the single crystal on commercial UV chips (300 nm) with glue. The electro-optical characteristics of LEDs, including voltage-luminance, electroluminescent (EL) spectra, CIE (x,y) coordinates, CRI, CCT and deviation of devices were measured and recorded by a computer-controlled power source (Keithley 2400 sourcemeter, USA) and spectrometer (PR-670, USA) The AC signal generated by an arbitrary waveform generator (Rigol DG4102, China), was combined with 8 V DC bias via a bias-T (Mini-Circuits Bias-Tee ZFBT-6GW+, USA), and the output signal was loaded into the LEDs. Amplified photodetector (PDA36A2) with a -3 dB bandwidth of 10 MHz was employed to convert photoelectric signals, and the resultant electrical signal was recorded by a digital storage oscilloscope (LeCroy WaveSurfer 432, USA).

ACKNOWLEDGMENTS

B.Q. Wang and C. Chen contributed equally to this work. This work is funded by Fundamental Research Funds for the Central Universities (2021CDJQY-022); National Natural Science Foundation of China (Nos. 61904023, 11974063); Natural Science Foundation of Chongqing

(No. cstc2019jcyj-bshX0078). The authors would like to thank Chuanyao Yang and Shijuan Xiao at Analytical and Testing Center of Chongqing University for their assistance with PL and XRD analysis.

CONFLICT OF INTEREST

The authors declare no conflict of interest.

ORCID

Zhigang Zang  <https://orcid.org/0000-0003-1632-503X>

REFERENCES

- Liu XK, Xu WD, Bai S, et al. Metal halide perovskites for light-emitting diodes. *Nat Mater*. 2021;20(1):10-21.
- Zhao SY, Zhang YB, Zang ZG. Room-temperature doping of ytterbium into efficient near-infrared emission CsPbBr_{1.5}Cl_{1.5} perovskite quantum dots. *Chem Commun*. 2020;56(43):5811-5814.
- Zhang YX, Liu YC, Xu Z, et al. Nucleation-controlled growth of superior lead-free perovskite Cs₃Bi₂I₉ single-crystals for high-performance X-ray detection. *Nat Commun*. 2020;11(1):2304.
- Mo QH, Chen C, Cai WS, Zhao SY, Yan DD, Zang ZG. Room temperature synthesis of stable zirconia-coated CsPbBr₃ nanocrystals for white light-emitting diodes and visible light communication. *Laser & Photonics Reviews*. 2021;15(10):2100278. <https://doi.org/10.1002/lpor.202100278>
- Yan DD, Zhao SY, Zhang YB, Wang HX, Zang ZG. Highly efficient emission and high-CRI warm white light-emitting diodes from ligand-modified CsPbBr₃ quantum dots. *Opto-Electronic Advances*. 2021;4:200075. <http://doi.org/10.29026/oea.2021.200075>
- Li XW, Cai WS, Guan HL, et al. Highly stable CsPbBr₃ quantum dots by silica-coating and ligand modification for white light-emitting diodes and visible light communication. *Chem Eng J*. 2021;419:129551.
- Mo QH, Shi TC, Cai WS, et al. Room temperature synthesis of stable silica-coated CsPbBr₃ quantum dots for amplified spontaneous emission. *Photonics Res*. 2020;8(10):1605-1612.
- Yan DD, Shi TC, Zang ZG, et al. Ultrastable CsPbBr₃ perovskite quantum dot and their enhanced amplified spontaneous emission by surface ligand modification. *Small*. 2019;15(23):1901173.
- Wei W, Zhang Y, Xu Q, et al. Monolithic integration of hybrid perovskite single crystals with heterogenous substrate for highly sensitive X-ray imaging. *Nat Photon*. 2017;11(5):315-321.
- Zhang HJ, Xu YD, Sun QH, et al. Lead free halide perovskite Cs₃Bi₂I₉ bulk crystals grown by a low temperature solution method. *CrstEngComm*. 2018;20(34):4935-4941.
- Niu TT, Chao LF, Gao WY, et al. Ionic liquids-enabled efficient and stable perovskite photovoltaics: progress and challenges. *ACS Energy Lett*. 2021;6(4):1453-1479.
- Jun T, Handa T, Sim K, et al. One-step solution synthesis of white-light-emitting films via dimensionality control of the Cs-Cu-I system. *APL Mater*. 2019;7(11):111113.
- Vashishtha P, Nutan GV, Griffith BE, et al. Cesium copper iodide tailored nanoplates and nanorods for blue, yellow, and white emission. *Chem Mater*. 2019;31(21):9003-9011.
- Luo JJ, Wang XM, Li SR, et al. Efficient and stable emission of warm-white light from lead-free halide double perovskites. *Nature*. 2018;563(7732):541-545.
- Ma JL, Xia XC, Yan S, et al. Stable and self-powered solar-blind ultraviolet photodetectors based on a Cs₃Cu₂I₅/beta-Ga₂O₃ heterojunction prepared by dual-source vapor codeposition. *ACS Appl Mater Interfaces*. 2021;13(13):15409-15419.
- Luo JJ, Li SR, Wu HD, et al. Cs₂AgInCl₆ double perovskite single crystals: parity forbidden transitions and their application for sensitive and fast UV photodetectors. *ACS Photon*. 2017;5(2):398-405.
- Zheng Z, Hu QS, Zhou HZ, et al. Submillimeter and lead-free Cs₃Sb₂Br₉ perovskite nanoflakes: inverse temperature crystallization growth and application for ultrasensitive photodetectors. *Nanosc Horiz*. 2019;4(6):1372-1379.
- Zhou JE, An K, He P, et al. Solution-processed lead-free perovskite nanocrystal scintillators for high-resolution X-ray CT imaging. *Adv Opt Mater*. 2021;9(11):2002144.
- Heo JH, Shin DH, Park JK, Kim DH, Lee SJ, Im SH. High-performance next-generation perovskite nanocrystal scintillator for nondestructive X-ray imaging. *Adv Mater*. 2018;30(40):1801743.
- Chen QS, Wu J, Ou XY, et al. All-inorganic perovskite nanocrystal scintillators. *Nature*. 2018;561(7721):88-93.
- Grandhi GK, Viswanath NSM, Cho HB, et al. Mechanochemistry as a green route: synthesis, thermal stability, and post-synthetic reversible phase transformation of highly-luminescent cesium copper halides. *J Phys Chem Lett*. 2020;11(18):7723-7729.
- Li ZQ, Li ZL, Shi ZF, Fang X. Facet-dependent, fast response, and broadband photodetector based on highly stable all-inorganic CsCu₂I₃ single crystal with 1D electronic structure. *Adv Funct Mater*. 2020;30(28):2002634.
- Zhao SY, Cai WS, Wang HX, Zang Z, Chen J. All-inorganic lead-free perovskite(-like) single crystals: synthesis, properties, and applications. *Small Methods*. 2021;5(5):2001308.
- Mo XM, Li T, Huang FC, et al. Highly-efficient all-inorganic lead-free 1D CsCu₂I₃ single crystal for white-light emitting diodes and UV photodetection. *Nano Energy*. 2021;81:105570.
- Zhao SY, Chen C, Cai WS, et al. Efficiently luminescent and stable lead-free Cs₃Cu₂Cl₅@silica nanocrystals for white light-emitting diodes and communication. *Adv Opt Mater*. 2021;9(13):2100307.
- Ma ZZ, Shi ZF, Yang DW, et al. High color-rendering index and stable white light-emitting diodes by assembling two broadband emissive self-trapped excitons. *Adv Mater*. 2021;33(2):2001367.
- Fang SF, Wang Y, Li HX, et al. Rapid synthesis and mechanochemical reactions of cesium copper halides for convenient chromaticity tuning and efficient white light emission. *J Mater Chem C*. 2020;8(14):4895-4901.
- Li Y, Shi ZF, Wang LT, et al. Solution-processed one-dimensional CsCu₂I₃ nanowires for polarization-sensitive and flexible ultraviolet photodetectors. *Mater Horiz*. 2020;7(6):1613-1622.
- Jun T, Sim K, Iimura S, et al. Lead-free highly efficient blue-emitting Cs₃Cu₂I₅ with 0D electronic structure. *Adv Mater*. 2018;30(43):1804547.
- Lin RC, Guo QL, Zhu Q, Zhu Y, Zheng W, Huang F. All-inorganic CsCu₂I₃ single crystal with high-PLQY (approximately 15.7%) intrinsic white-light emission via strongly localized 1D excitonic recombination. *Adv Mater*. 2019;31(46):1905079.
- Creason TD, McWhorter TM, Bell Z, et al. K₂CuX₃ (X = Cl, Br): All-inorganic lead-free blue emitters with near-unity photoluminescence quantum yield. *Chem Mater*. 2020;32(14):6197-6205.
- Wang XD, Li WG, Liao JF, Kuang DB. Recent advances in halide perovskite single-crystal thin films: fabrication methods and optoelectronic applications. *Sol RRL*. 2019;3(4):1800294.

33. Yin LX, Wu HD, Pan WC, et al. Controlled cooling for synthesis of $\text{Cs}_2\text{AgBiBr}_6$ single crystals and its application for X-ray detection. *Adv Opt Mater*. 2019;7(19):1900451.
34. Zhang MY, Zhu JS, Yang B, et al. Oriented-structured CsCu_2I_3 film by close-space sublimation and nanoscale seed screening for high-resolution X-ray imaging. *Nano Lett*. 2021;21(3):1392-1399.
35. Di JY, Chang JJ, Liu SZ. Recent progress of two-dimensional lead halide perovskite single crystals: crystal growth, physical properties, and device applications. *ECOMAT*. 2020;2(3):1-24.
36. Cheng PF, Sun L, Feng L, et al. Colloidal synthesis and optical properties of all-inorganic low-dimensional cesium copper halide nanocrystals. *Angew Chem Int Ed*. 2019;58(45):16087-16091.
37. Du MH. Emission trend of multiple self-trapped excitons in luminescent 1D copper halides. *ACS Energy Lett*. 2020;5(2):464-469.
38. Li Q, Chen ZW, Yang B, et al. Pressure-induced remarkable enhancement of self-trapped exciton emission in one-dimensional CsCu_2I_3 with tetrahedral units. *J Am Chem Soc*. 2020;142(4):1786-1791.
39. Kentsch R, Morgenroth M, Scholz M, et al. Direct observation of the exciton self-trapping process in CsCu_2I_3 thin films. *J Phys Chem Lett*. 2020;11(11):4286-4291.
40. Jing YY, Liu Y, Jiang XX, Molokeev MS, Lin Z, Xia Z. Sb^{3+} dopant and halogen substitution triggered highly efficient and tunable emission in lead-free metal halide single crystals. *Chem Mater*. 2020;32(12):5327-5334.
41. Wang BQ, Kou ZQ, Yuan QS, Fu X', Fan Z, Zhou A. Improving CRI of white phosphorescence organic light-emitting diodes by controlling exciton energy transfer in the planar heterojunction. *Org Electron*. 2020;78:105617.
42. Guan HL, Zhao SY, Wang HX, Yan D, Wang M, Zang Z. Room temperature synthesis of stable single silica-coated CsPbBr_3 quantum dots combining tunable red emission of Ag-In-Zn-S for high-CRI white light-emitting diodes. *Nano Energy*. 2020;67:104279.
43. Liu ZQ, Zhang YQ, Fan Y, et al. Toward highly luminescent and stabilized silica-coated perovskite quantum dots through simply mixing and stirring under room temperature in air. *ACS Appl Mater Interfaces*. 2018;10(15):13053-13061.
44. He QY, Zhang YQ, Yu YX, et al. Ultrastable Gd^{3+} doped CsPbBr_2I nanocrystals red glass for high efficiency WLEDs. *Chem Eng J*. 2021;411:128530.
45. Sun R, Lu P, Zhou DL, et al. Samarium-doped metal halide perovskite nanocrystals for single-component electroluminescent white light-emitting diodes. *ACS Energy Lett*. 2020;5(7):2131-2139.
46. Gao ZY, Wang XY, Bai YF, et al. High color rendering index and stable white light emitting diodes fabricated from lead bromide perovskites. *Appl Phys Lett*. 2019;115(15):153103.
47. Mao LL, Wu YL, Stoumpos CC, Wasielewski MR, Kanatzidis MG. White-light emission and structural distortion in new corrugated two-dimensional lead bromide perovskites. *J Am Chem Soc*. 2017;139(14):5210-5215.
48. Dohner ER, Jaffe A, Bradshaw LR, Karunadasa HI. Intrinsic white-light emission from layered hybrid perovskites. *J Am Chem Soc*. 2014;136(38):13154-13157.
49. Wang AF, Guo YY, Zhou ZB, et al. Aqueous acid-based synthesis of lead-free tin halide perovskites with near-unity photoluminescence quantum efficiency. *Chem Sci*. 2019;10(17):4573-4579.
50. Shao H, Wu XF, Zhu JY, et al. Mn^{2+} ions doped lead-free zero-dimensional K_3SbCl_6 perovskite. *Chem Eng J*. 2021;413:127415.
51. Zhao SY, Mo QH, Cai WS, Wang H, Zang Z. Inorganic lead-free cesium copper chlorine nanocrystal for highly efficient and stable warm white light-emitting diodes. *Photonics Res*. 2021;9(2):187-192.
52. Zhou CK, Lin HR, Tian Y, et al. Luminescent zero-dimensional organic metal halide hybrids with near-unity quantum efficiency. *Chem Sci*. 2018;9(3):586-593.
53. Deng W, Jin XC, Lv Y, Zhang X, Zhang X, Jie J. 2D ruddlesden-popper perovskite nanoplate based deep-blue light-emitting diodes for light communication. *Adv Funct Mater*. 2019;29(40):1903861.
54. Chen C, Zhong WD, Wu DH. Indoor OFDM visible light communications employing adaptive digital pre-frequency domain equalization. *Conf Lasers Electro-Opt (CLEO)*. 2016;JTh2A.118.

SUPPORTING INFORMATION

Additional supporting information may be found in the online version of the article at the publisher's website.

How to cite this article: Wang B, Chen C, Yang X, et al. Pressure-assisted cooling to grow ultra-stable $\text{Cs}_3\text{Cu}_2\text{I}_5$ and CsCu_2I_3 single crystals for solid-state lighting and visible light communication. *EcoMat*. 2022;4(2):e12184. doi:10.1002/eom2.12184